FUDMA Journal of Sciences (FJS)
ISSN online: 2616-1370
ISSN print: 2645 - 2944
Vol. 10 No. 22, November, 2026, pp 307 – 320
DOI: https://doi.org/10.33003/fjs-2026-1022-5780

Transient Double-Diffusive Convection in a Vertical Channel with Soret–Dufour Effects, Viscous Dissipation, Heat Generation and Chemical Reaction

***[1]Isaac Adaji, [1]Danjuma Yahaya Jibrin, [1]Ibrahim Aminu, [2]Rasaq Oyeyemi Olayiwola, [1]Aishat Oyiza Musa, [1]Raji Muhammed, [3]Danjuma Abdul Yusuf and [1]Aniki S. A.**

[1]Mathematic and Statistics Department, Confluence University of Science and Technology, Osara, Kogi State, Nigeria.
[2]Mathematic and Statistics Department, Federal University of Technology, Minna, Niger State, Nigeria.
[3]Acturial Science Department, Confluence University of Science and Technology, Osara, Kogi State, Nigeria

*Corresponding authors' email: isaacadaji4real@gmail.com Phone: +2348131662362
ORCID: https://orcid.org/0009-0005-0605-8224

Received: 20 Aug. 2026
Accepted: 21 Oct. 2026
Published: 03 Nov. 2026

ABSTRACT
This paper investigates transient double-diffusive free convection flow in a vertical channel, incorporating the combined effects of Soret and Dufour cross-diffusion, viscous dissipation, internal heat generation/absorption, and first-order chemical reaction. The governing equations for momentum, energy, and species concentration are formulated under the Boussinesq approximation and non-dimensionalized to identify the key governing parameters: Prandtl number, Schmidt number, Dufour number, Soret number, Eckert number, buoyancy ratio, heat source parameter, chemical reaction parameter, Reynolds number, and thermal Grashof number. Analytical solutions are obtained using Olayiwola's Generalized Polynomial Approximation Method (OGPAM), a robust technique for solving parabolic partial differential equations with constant or variable coefficients. The solutions are validated against numerical results computed via Maple 2015's Dsolve numeric function, with excellent agreement confirming the accuracy and reliability of the analytical approach. The results demonstrate that increasing the Dufour and Soret numbers enhances temperature, concentration, and velocity fields through cross-diffusion mechanisms, while viscous dissipation substantially increases temperature and velocity in high-velocity flows. The Prandtl number reduces temperature, velocity, Nusselt number, and skin friction, but enhances species concentration and Sherwood number. The Schmidt number reduces all transport quantities, whereas the thermal Grashof number enhances temperature and velocity through strengthened buoyancy. The chemical reaction parameter significantly reduces species concentration, acting as a sink for the concentration field. The heat generation/absorption parameter reduces temperature while increasing concentration, revealing complex coupling between thermal and concentration fields. These findings have direct relevance to practical applications including isotope separation, cooling of vertical printed circuit boards, geothermal system design, chemical processing equipment, and environmental management systems. The analytical solutions provide efficient tools for parametric studies and system optimization in double-diffusive transport processes

Keywords: Transient Flow, Double-Diffusive Convection, Vertical Channel, Dufour Effect, Soret Effect, OGPAM

INTRODUCTION

The study of fluid flow through vertical channels represents a fundamental area of investigation in fluid dynamics, with extensive applications spanning hydraulic engineering, environmental science, and industrial processes. Understanding transient flow behavior where fluid parameters vary with time in response to changing boundary conditions or external forces is critical for designing efficient drainage systems, flood management infrastructure, wastewater treatment facilities, and industrial reactors (Nash & Morris, 2018; Meyer & Rogers, 2022). Unlike steady-state conditions where velocity and pressure remain constant, transient flows exhibit dynamic variations that must be accurately modeled to predict system performance under real-world operational scenarios.

In vertical channel configurations, gravitational effects play a dominant role, and the modeling framework must account for buoyancy-driven forces arising from both thermal and concentration gradients. The Boussinesq approximation, which assumes density variations are negligible except in buoyancy terms, provides a widely adopted foundation for analyzing such flows (Chanson, 2020). Recent advancements in computational fluid dynamics (CFD) have significantly enhanced our ability to simulate complex transient flow patterns, enabling detailed investigations of turbulence, variable channel geometries, and coupled transport phenomena (Patankar, 2020).

The simultaneous transfer of heat and mass in fluid systems termed double-diffusive convection occurs in numerous engineering applications including fire engineering, combustion modeling, nuclear energy systems, petroleum reservoirs, heat exchangers, solar panels, building ventilation systems, and chemical distilleries (Ismael *et al.,* 2014; Umavathi & Sheremet, 2016; Umavathi *et al.*, 2016; Yahaya *et al.*, 2025). Two particularly important cross-diffusion phenomena in such systems are the Dufour effect (diffusion-

thermo), where a concentration gradient generates a heat flux, and the Soret effect (thermal diffusion), where a temperature gradient drives mass transport. Although these effects are typically smaller in magnitude compared to Fourier's and Fick's law contributions, they become significant in applications involving isotope separation and mixing of gases with dissimilar molecular weights (Alam *et al.*, 2007).

Viscous energy dissipation, arising from the conversion of mechanical energy into thermal energy through fluid friction, represents another important mechanism influencing temperature fields in high-velocity or high-viscosity flows. Additionally, internal heat generation or absorption, chemical reactions, and thermal radiation further complicate the transport phenomena. Despite extensive research on transient flows in various configurations, limited studies have comprehensively addressed the combined influence of Dufour effect, Soret effect, viscous dissipation, heat generation/absorption, and chemical reaction in vertical channel flows.

This paper develops a mathematical model for transient double-diffusive free convection flow in a vertical channel, incorporating the aforementioned effects under the Boussinesq approximation. The governing equations are solved using Olayiwola's Generalized Polynomial Approximation Method (OGPAM), a robust analytical technique for parabolic partial differential equations (Olayiwola, 2022). The study aims to:

(i) Develop a comprehensive mathematical model for transient free convectional flow through a vertical channel governed by Dufour and Soret effects under the Boussinesq approximation;

(ii) Obtain analytical solutions for velocity, temperature, and concentration fields using OGPAM;

(iii) Investigate the influence of key dimensionless parameters on flow characteristics and transport coefficients.

MATERIALS AND METHODS

Olayiwola's Generalized Polynomial Approximation Method (OGPM)

Polynomial approximation methods are widely utilized for obtaining approximate solutions to partial differential equations in mathematical physics. A significant advancement in this area is the development of Olayiwola's Generalized Polynomial Approximation Method (OGPAM), which extends traditional polynomial techniques. OGPAM is capable of solving parabolic equations with either constant or variable coefficients across various geometries, including slab, cylindrical, and spherical configurations (Olayiwola, 2022). The method involves five steps. The steps are applied to the dimensionless governing equation as shown below:

The parabolic equations are defined by

$$\frac{\partial \varphi}{\partial t} = \frac{k}{r^n}\frac{\partial}{\partial r}\left(r^n \frac{\partial \varphi}{\partial r}\right) + F(r,t,\varphi), t > 0,$$
$$r \in \Omega(\Omega \subset R^1, R^2 or R^3) \quad (1)$$

with the initial condition

$$\varphi(r,0) = f(r) \quad (2)$$

and the boundary conditions

$$\alpha_1 \frac{\partial \varphi}{\partial r}\Big|_{r=a} + \beta_1 \varphi|_{r=a} = g_1(t), \alpha_2 \frac{\partial \varphi}{\partial r}\Big|_{r=b} + \beta_2 \varphi|_{r=b} = g_2(t) \quad (3)$$

where $F(r,t,\varphi)$ are the other terms in equation (1), $n = 0$ for a slab, $n = 1$ for cylinder, $n = 2$ for sphere, $f(r), g_1(t), g_2(t)$ are three known functions, $n, k, \alpha_1, \alpha_2, \beta_1, \beta_2$ are constants, and $a \le r \le b$ is the boundary of Ω.

To obtain an approximate solution of the partial differential equation (1) satisfying (2) and (3), the following steps are involved:

Case 1: When $\alpha_1 \neq 0$ and $\alpha_2 = 0$

Step 1: Compare the equation to be solved with equations (1) – (3) and obtain A, B, C and $F(r,t,\varphi)$ where

$$A = \begin{pmatrix} \frac{b(b-2a)}{b(b-2a)+a^2}\left(1+\frac{a}{\alpha_1}\left(1+\frac{a}{(b-2a)}\right)\beta_1\right) - \\ \frac{(n+1)(b^{n+2}-a^{n+2})}{(n+2)(b^{n+1}-a^{n+1})}\left(\frac{\beta_1}{\alpha_1}+\frac{2a}{(b-2a)}\frac{\beta_1}{\alpha_1} - \frac{2a}{b(b-2a)+a^2}\left(1+\frac{a}{\alpha_1}\left(1+\frac{a}{(b-2a)}\right)\beta_1\right)\right) + \\ \frac{(n+1)(b^{n+3}-a^{n+3})}{(n+3)(b^{n+1}-a^{n+1})}\left(\frac{\beta_1}{(b-2a)\alpha_1} - \frac{1}{b(b-2a)+a^2}\left(1+\frac{a}{\alpha_1}\left(1+\frac{a}{(b-2a)}\right)\beta_1\right)\right) \end{pmatrix}$$

$$B = \begin{pmatrix} -\frac{ab(b-2a)}{(b(b-2a)+a^2)\alpha_1}\left(1+\frac{a}{(b-2a)}\right) + \\ \frac{(n+1)(b^{n+2}-a^{n+2})}{(n+2)(b^{n+1}-a^{n+1})}\left(\frac{1}{\alpha_1}+\frac{2a}{(b-2a)\alpha_1} - \frac{2a^2}{(b(b-2a)+a^2)\alpha_1}\left(1+\frac{a}{(b-2a)}\right)\right) + \\ \frac{(n+1)(b^{n+3}-a^{n+3})}{(n+3)(b^{n+1}-a^{n+1})}\left(\frac{a}{(b(b-2a)+a^2)\alpha_1}\left(1+\frac{a}{(b-2a)}\right) - \frac{1}{(b-2a)\alpha_1}\right) \end{pmatrix}$$

$$C = \begin{pmatrix} \frac{a^2}{(b(b-2a)+a^2)} - \frac{(n+1)(b^{n+2}-a^{n+2})}{(n+2)(b^{n+1}-a^{n+1})}\frac{2a}{b(b-2a)\beta_2}\left(1-\frac{a^2}{(b(b-2a)+a^2)}\right) + \\ \frac{(n+1)(b^{n+3}-a^{n+3})}{(n+3)(b^{n+1}-a^{n+1})}\frac{1}{b(b-2a)\beta_2}\left(1-\frac{a^2}{(b(b-2a)+a^2)}\right) \end{pmatrix}$$

Step 2: Assume Olayiwola's generalized polynomial solution:

$$\varphi(r,t)=\begin{pmatrix}\left(\frac{b(b-2a)}{b(b-2a)+a^2}\right)\begin{pmatrix}\left(1+\frac{a}{\alpha_1}\left(1+\frac{ab}{b(b-2a)}\right)\beta_1\right)\varphi|_{r=a}-\frac{a}{\alpha_1}\left(1+\frac{ab}{b(b-2a)}\right)g_1\\+\left(\frac{a^2}{b(b-2a)\beta_2}\right)g_2\end{pmatrix}+\\\begin{pmatrix}\left(\frac{2a}{b(b-2a)}\left(\frac{b(b-2a)}{b(b-2a)+a^2}\right)\left(1+\frac{a}{\alpha_1}\left(1+\frac{ab}{b(b-2a)}\right)\beta_1\right)-\\\frac{2a\beta_1}{(b-2a)\alpha_1}-\frac{\beta_1}{\alpha_1}\end{pmatrix}\varphi|_{r=a}+\\\left(\frac{1}{\alpha_1}+\frac{2a}{(b-2a)\alpha_1}-\frac{2a^2}{b(b-2a)\alpha_1}\left(\frac{b(b-2a)}{b(b-2a)+a^2}\right)\left(1+\frac{ab}{b(b-2a)}\right)\right)g_1\\+\left(\frac{2a}{b(b-2a)}\left(\frac{b(b-2a)}{b(b-2a)+a^2}\right)\left(\frac{a^2}{b(b-2a)\beta_2}\right)-\left(\frac{2a}{b(b-2a)\beta_2}\right)\right)g_2\end{pmatrix}r+\\\frac{1}{b(b-2a)}\begin{pmatrix}\left(\frac{b\beta_1}{\alpha_1}-\left(\frac{b(b-2a)}{b(b-2a)+a^2}\right)\left(1+\frac{a}{\alpha_1}\left(1+\frac{ab}{b(b-2a)}\right)\beta_1\right)\right)\varphi|_{r=a}+\\\left(\left(\frac{b(b-2a)}{b(b-2a)+a^2}\right)\frac{a}{\alpha_1}\left(1+\frac{ab}{b(b-2a)}\right)-\frac{b}{\alpha_1}\right)g_1+\\\left(\frac{1}{\beta_2}-\left(\frac{b(b-2a)}{b(b-2a)+a^2}\right)\left(\frac{a^2}{b(b-2a)\beta_2}\right)\right)g_2\end{pmatrix}r^2\end{pmatrix} \quad (4)$$

Step 3: By using (4), evaluate

$$\frac{(n+1)}{(b^{n+1}-a^{n+1})}\int_a^b r^n F(r,t,\varphi)\,dr \quad (5)$$

and express the result in the form:

$$p_1\varphi|_{r=b}+q_1(t) \quad (6)$$

Step 4: Obtain p_1 and $q_1(t)$

Step 5: Obtain

$$\varphi|_{r=a}=e^{-\int p(t)dt}\int_0^t q(x)\,e^{\int p(x)dx}dx+f(r)e^{-\int p(t)dt} \quad (7)$$

where

$$p(t)=\frac{1}{A}\left(\frac{k(n+1)}{(b^{n+1}-a^{n+1})}\left(\frac{(b^n-a^n)\beta_1}{\alpha_1}+\frac{2b^n(a-b)}{(b-2a)\alpha_1}+\frac{2b^n(b-a)}{(b(b-2a)+a^2)}+\frac{2ab^n(b-a)(b(b-2a)+a)\beta_1}{(b(b-2a)+a^2)b(b-2a)\alpha_1}\right)-p_1\right)$$

$$q(t)=\frac{1}{A}\left(\frac{k(n+1)}{(b^{n+1}-a^{n+1})}\left(\frac{(b^n-a^n)}{\alpha_1}+\frac{2b^n(a-b)}{(b-2a)\alpha_1}+\frac{2ab^n(b-a)(b(b-2a)+a)}{(b(b-2a)+a^2)b(b-2a)\alpha_1}\right)g_1+\frac{k(n+1)}{(b^{n+1}-a^{n+1})}\frac{2b^n(b-a)}{b(b-2a)\beta_2}\left(1+\frac{a^2}{(b(b-2a)+a^2)}\right)g_2+q_1(t)-B\frac{\partial g_1}{\partial t}-C\frac{\partial g_2}{\partial t}\right)$$

Mathematical Formulation

Governing Equations

Consider transient free convection flow of a viscous, incompressible fluid through a vertical channel formed by two infinite parallel plates separated by distance L. The $x'-axis$ is taken along the vertical direction, while the $y'-axis$ is normal to the channel walls. Initially, both the fluid and the channel walls are at rest with constant temperature T_L' and concentration C_L'. Due to the infinite length of the walls, all physical quantities depend only on y' and time t'.

Under the Boussinesq approximation, the governing equations for momentum, energy, and species concentration, incorporating viscous dissipation, Dufour effect, Soret effect, heat generation, and chemical reaction, are:

Momentum Equation

$$\frac{\partial u'}{\partial t'}=v\frac{\partial^2 u'}{\partial y'^2}+g\beta(T'-T_0')+g\beta^*(C'-C_0') \quad (8)$$

Energy Equation

$$\frac{\partial T'}{\partial t'}=\alpha\frac{\partial^2 T'}{\partial y'^2}+D^*\frac{\partial^2 C'}{\partial y'^2}+\frac{v}{c_p}\left(\frac{\partial u'}{\partial y'}\right)^2+\frac{Q^*}{\rho c_p}(T'-T_0') \quad (9)$$

Species Concentration Equation

$$\frac{\partial C'}{\partial t'}=D_m\frac{\partial^2 C'}{\partial y'^2}+K^*\frac{\partial^2 T'}{\partial y'^2}-K^*{}_c(C'-C_0') \quad (10)$$

The initial and boundary conditions for symmetric heating and consumption at wall $y'=0$ with no-slip at wall $y'=L$ are:

$$\left.\begin{aligned}&u'(y',0)=0, \quad \left.\frac{\partial u'}{\partial y'}\right|_{y'=0}=0, \quad u'(L,t)=0\\&T'(y',0)=T_L', \quad \left.\frac{\partial T'}{\partial y'}\right|_{y'=0}=0, \quad T'(L,t)=T_L'\\&C'(y',0)=C_L', \quad \left.\frac{\partial C'}{\partial y'}\right|_{y'=0}=0, \quad C'(L,t)=C_L'\end{aligned}\right\} \quad (11)$$

Non-Dimensionalization

The following dimensionless quantities are introduced:

$$\left.\begin{aligned}&t=\frac{t'}{t_0}, \quad t_0=\frac{L^2}{v}, \quad y=\frac{y'}{L}, \quad u=\frac{vu'}{g\beta(T_L'-T_0')L^2},\\&\theta=\frac{T'-T_0}{T_L'-T_0'}, \quad \phi=\frac{C'-C_0'}{C_L'-C_0'}\end{aligned}\right\} \quad (12)$$

Applying these transformations yields the dimensionless governing equations:

Momentum

$$\frac{\partial u}{\partial t} = \frac{\partial^2 u}{\partial y^2} + \theta + N\phi \quad (13)$$

where $N = \frac{Gr\phi}{Gr\theta} = \frac{g\beta^*(C_L' - C_0')}{g\beta(T_L' - T_0')}$ is the buoyancy ratio.

Energy

$$\frac{\partial \theta}{\partial t} = \frac{1}{P_r}\frac{\partial^2 \theta}{\partial y^2} + D_f \frac{\partial^2 \phi}{\partial y^2} + \frac{E_c G^2 r_\theta}{Re^2}\left(\frac{\partial u}{\partial y}\right)^2 + Q\theta \quad (14)$$

Species Concentration

$$\frac{\partial \phi}{\partial t} = \frac{1}{S_c}\frac{\partial^2 \phi}{\partial y^2} + S_r \frac{\partial^2 \theta}{\partial y^2} - K_r\phi \quad (15)$$

The dimensionless initial and boundary conditions become:

$$\left.\begin{array}{llll} u(y,\,0) = 0 & \left.\frac{\partial u}{\partial y}\right|_{y=0} = 0, & u(1,\,t) = 0 \\ \theta(y,\,0) = 1 & \left.\frac{\partial \theta}{\partial y}\right|_{y=0} = 0, & \theta(1,\,t) = 1 \\ \phi(y,\,0) = 1 & \left.\frac{\partial \phi}{\partial y}\right|_{y=0} = 0, & \phi(1,\,t) = 1 \end{array}\right\} \quad (16)$$

where the dimensionless parameters are defined as:

$S_c = \frac{\nu}{D_m}$ (Schmidt number)

$K_r = \frac{K_c^* L^2}{\nu}$ (Chemical reaction parameter)

$S_r = \frac{D_m K_T (T_L' - T_0')}{T_m (C_L' - C_0')\nu}$ (Soret number)

$P_r = \frac{\nu}{\alpha}$ (Prandtl number)

$D_f = \frac{D_m K_T (C_L' - C_0')}{C_s C_P (T_L' - T_0')\nu}$ (Dufour number)

$Q = \frac{Q^* L^2}{\rho C_p \nu}$ (Heat source parameter)

$E_c = \frac{U^2}{C_P (T_L' - T_0')}$ (Eckert number)

$Gr_\theta = \frac{g\beta(T_L' - T_0')L^3}{\nu^2}$ (Thermal Grashof number

$R_e = \frac{LU}{\nu}$ (Reynolds number)

METHOD OF SOLUTION

Perturbation Expansion

Since the equations are coupled, we let $0 < N << 1$, $E_c = aN$, $S_r = bN$, such that we can express

$$\left.\begin{array}{l} u(y,\,t) = u_0(y,\,t) + Nu_1(y,\,t) \\ \theta(y,\,t) = \theta_0(y,\,t) + N\theta_1(y,\,t) \\ \phi(y,\,t) = \phi_0(y,\,t) + N\phi_1(y,\,t) \end{array}\right\} \quad (17)$$

Substituting (10) into (6)-(8) and collecting terms of order N^0 and N^1 yields two sets of linearized equations.

Zeroth-Order Equations N^0

Concentration

$$\left.\begin{array}{l} \frac{\partial \phi_0}{\partial t} = \frac{1}{S_c}\frac{\partial^2 \phi_0}{\partial y^2} - K_r\phi_0 \\ \phi_0(y,\,0) = 1, \quad \left.\frac{\partial \phi_0}{\partial y}\right|_{y=0} = 0 \quad \phi_0(1,\,t) = 1 \end{array}\right\} \quad (18)$$

Energy

$$\left.\begin{array}{l} \frac{\partial \theta_0}{\partial t} = \frac{1}{P_r}\frac{\partial^2 \theta_0}{\partial y^2} + D_f \frac{\partial^2 \phi_0}{\partial y^2} + Q\theta_0 \\ \theta_0(y,\,0) = 1, \quad \left.\frac{\partial \theta_0}{\partial y}\right|_{y=0} = 0 \quad \theta_0(1,\,t) = 1 \end{array}\right\} \quad (19)$$

Momentum

$$\left.\begin{array}{l} \frac{\partial u_0}{\partial t} = \frac{\partial^2 u_0}{\partial y^2} + \theta_0 \\ u_0(y,\,0) = 0, \quad \left.\frac{\partial u_0}{\partial y}\right|_{y=0} = 0, \quad u_0(1,\,t) = 0 \end{array}\right\} \quad (20)$$

Solution for $(\boldsymbol{\theta_1})$

From equation (22):

$$\theta_1(y,t) = \theta_1|_{y=0}(1 - y^2) \quad (31)$$

First-Order Equations N^1

Concentration

$$\left.\begin{array}{l} \frac{\partial \phi_1}{\partial t} = \frac{1}{S_c}\frac{\partial^2 \phi_1}{\partial y^2} + b\frac{\partial^2 \theta_0}{\partial y^2} - K_r\phi_1 \\ \phi_1(y,\,0) = 0, \quad \left.\frac{\partial \phi_1}{\partial y}\right|_{y=0} = 0 \quad \phi_1(1,\,t) = 0 \end{array}\right\} \quad (21)$$

Energy

$$\left.\begin{array}{l} \frac{\partial \theta_1}{\partial t} = \frac{1}{P_r}\frac{\partial^2 \theta_1}{\partial y^2} + D_f \frac{\partial^2 \phi_1}{\partial y^2} + \frac{aG^2 r_\theta}{Re^2}\left(\frac{\partial u_0}{\partial y}\right)^2 + Q\theta_1 \\ \theta_1(y,\,0) = 0, \quad \left.\frac{\partial \theta_1}{\partial y}\right|_{y=0} = 0 \quad \theta_1(1,\,t) = 0 \end{array}\right\} \quad (22)$$

Momentum

$$\left.\begin{array}{l} \frac{\partial u_1}{\partial t} = \frac{\partial^2 u_1}{\partial y^2} + \theta_1 + \phi_0 \\ u_1(y,\,0) = 0, \quad \left.\frac{\partial u_1}{\partial y}\right|_{y=0} = 0, \quad u_1(1,\,t) = 0 \end{array}\right\} \quad (23)$$

Solution using OGPAM

Olayiwola's Generalized Polynomial Approximation Method (OGPAM) is employed to solve the parabolic equations. The method involves representing the solution as a polynomial in the spatial coordinate and reducing the partial differential equations to ordinary differential equations in time.

Solution for $(\boldsymbol{\phi_0})$

Comparing equation (18) with the standard parabolic form and applying OGPAM yields:

$$\phi_0(y,t) = \left(\frac{C_0}{K_r} + \left(1 - \frac{C_0}{K_r}\right)e^{-K_r t}\right)(1 - y^2) + y^2 \quad (24)$$

where $C_0 = \frac{3}{2}\left(\frac{2}{S_c} - \frac{K_r}{3}\right)$

Solution for $(\boldsymbol{\theta_0})$

Similarly, solving equation (19) gives:

$$\theta_0(y,t) = \theta_0|_{y=0}(1 - y^2) + y^2 \quad (25)$$

where:

$$\theta_0|_{y=0} = \left(\left(1 + \frac{C_1}{Q} - \frac{C_2}{Q + K_r}\right)e^{Qt} + \frac{C_2}{Q + K_r}e^{-K_r t} - \frac{C_1}{Q}\right) \quad (26)$$

And $C_1 = \frac{3}{2}\left(\frac{2}{p_r} + \frac{Q}{3} + 2D_f - \frac{2D_f C_0}{K_r}\right)$, $C_2 = 2D_f\left(1 - \frac{C_0}{K_r}\right)$

Solution for $(\boldsymbol{u_0})$

From equation (20):

$$u_0(y,t) = u_0|_{y=0}(1 - y^2) \quad (27)$$

where:

$$= C_3 t + \frac{C_4}{Q}(e^{Qt} - 1) - \frac{C_5}{K_r}(e^{-K_r t} - 1) \quad (28)$$

and $C_3 = \left(\frac{1}{2} - \frac{C_1}{Q}\right)$, $C_4 = \left(1 + \frac{C_1}{Q} - \frac{C_2}{Q + K_r}\right)$, $C_5 = \frac{C_2}{Q + K_r}$

Solution for $(\boldsymbol{\phi_1})$

Solving equation (21):

$$\phi_1(y,t) = \phi_1|_{y=0}(1 - y^2) \quad (29)$$

where:

$$\phi_1|_{y=0} = \frac{C_9}{K_r} - \frac{C_{10}}{Q + K_r}e^{Qt} + \left(\frac{C_{10}}{Q + K_r} - \frac{C_9}{K_r}\right)e^{-K_r t} - C_{11}te^{-K_r t} \quad (30)$$

with: $C_9 = 3b\left(1 - \frac{C_1}{Q}\right)$, $C_{10} = 3bC_4$, $C_{11} = 3bC_5$

where $\theta_1|_{y=0}$ is given by a combination of exponential and polynomial terms:

$$= C_{22} + C_{23}t + C_{24}t^2 + C_{25}e^{Qt} + C_{26}e^{-K_r t} + C_{27}te^{Qt} + C_{28}te^{-K_r t} + C_{29}t^2e^{Qt} + C_{30}e^{2Qt} + C_{31}e^{(Q-K_r)t} + C_{32}e^{-2K_r t} \quad (32)$$

The coefficients C_{12} through C_{32} are provided in the Appendix.

Solution for (u_1)

Finally, from equation (23):

$$u_1(y,t) = u_1|_{y=0}(1-y^2) \quad (33)$$

where:

$$u_1|_{y=0} = C_{33}t + \frac{C_{23}}{2}t^2 + \frac{C_{24}}{3}t^3 + \frac{C_{25}}{Q}(e^{Qt}-1) - \frac{C_{34}}{K_r}(e^{-K_r t}-1) - C_{28}\left(\frac{te^{-K_r t}}{K_r} + \frac{(e^{-K_r t}-1)}{{K_r}^2}\right) + \frac{C_{30}}{2Q}(e^{2Qt}-1) + \frac{C_{31}}{Q-K_r}(e^{(Q-K_r)t}-1) - \frac{C_{32}}{2K_r}(e^{-2K_r t}-1) + C_{27}\left(\frac{te^{Qt}}{Q} - \frac{(e^{Qt}-1)}{Q^2}\right) + C_{29}\left(\frac{t^2e^{Qt}}{Q} - \frac{2te^{Qt}}{Q^2} + \frac{2(e^{Qt}-1)}{Q^3}\right) \quad (34)$$

RESULTS AND DISCUSSION

Validation of Analytical Solutions

To validate the analytical solutions obtained via OGPAM, numerical solutions were computed using Maple 2015's Dsolve numeric function. Table 1 presents a comparison of the analytical and numerical results for temperature (θ), concentration (ϕ), and velocity (u) profiles at selected spatial locations for $N = 0.01$, $Pr = 0.71$, $Sc = 0.78$, $D_f = 0.06$, $Q = 1$, $K_r = 10$, $Ec = 1$, $S_r = 0.1$, $Re = 100$, $Gr_\theta = 0.1$, and $t = 0.8$.

Table 1: Comparison of Numerical and Analytical Solutions

y	Numerical Solution			Analytical Solution		
	u	θ	ϕ	u	θ	ϕ
0.00	0.398649	1.104726	0.977766	0.397345	1.104013	0.977782
0.10	0.393098	1.100827	0.978067	0.393371	1.102973	0.978004
0.20	0.376704	1.090184	0.978943	0.381451	1.099853	0.978671
0.30	0.350208	1.075421	0.980331	0.361584	1.094652	0.979782
0.40	0.314755	1.059512	0.982153	0.333769	1.087371	0.981337
0.50	0.271780	1.044687	0.984348	0.298008	1.078010	0.983337
0.60	0.222886	1.032012	0.986877	0.254301	1.066568	0.985781
0.70	0.169724	1.021606	0.989718	0.202646	1.053047	0.988669
0.80	0.113902	1.013104	0.992861	0.143044	1.037445	0.992002
0.90	0.056897	1.006033	0.996294	0.075495	1.019763	0.995779
1.00	0	1	1	0	1	1

The excellent agreement between analytical and numerical results confirms the accuracy and reliability of the OGPAM solutions

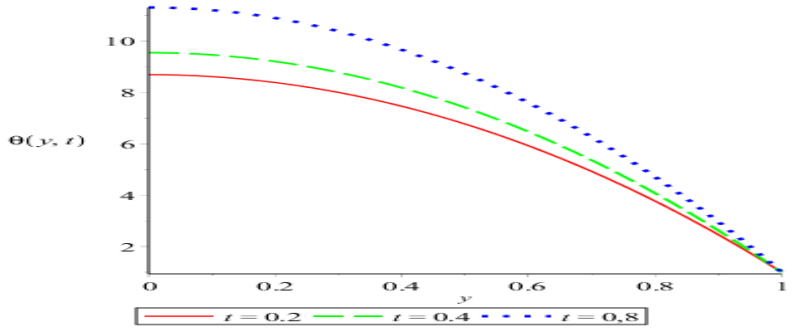


Figure 1: Temperature Profile for Various t

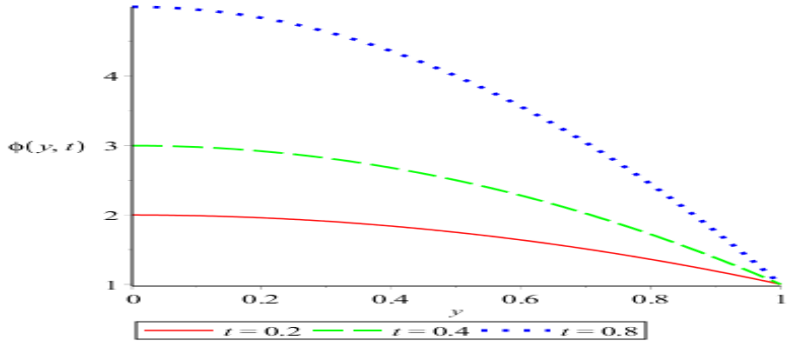


Figure 2: Concentration Profile for Various t

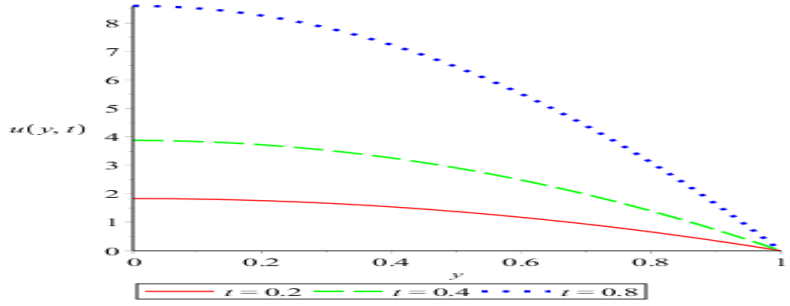


Figure 3: Velocity Profile for Various t.

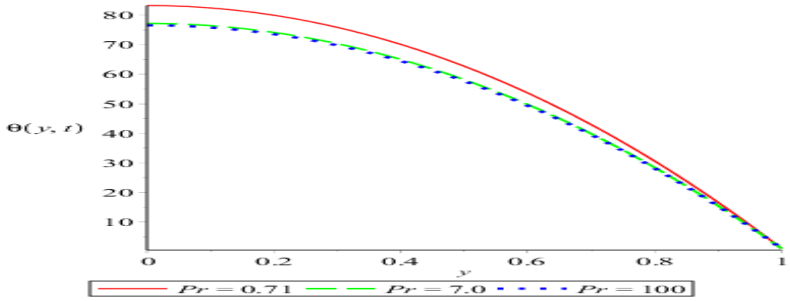


Figure 4: Prandtl Number Effect on the Temperature.

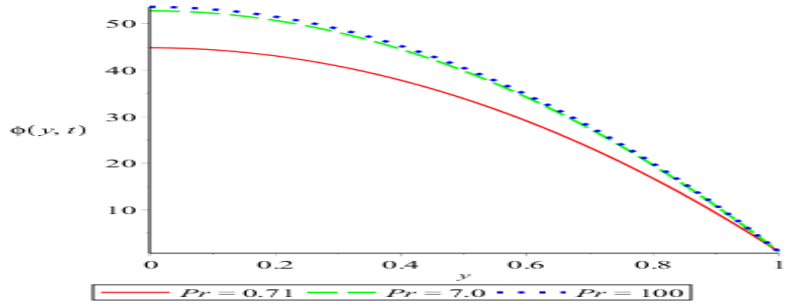


Figure 5: Prandtl Number Effect on the Concentration.

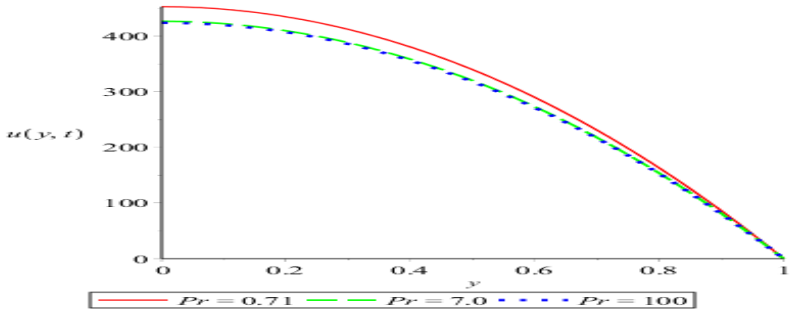


Figure 6: Prandtl Number Effect on the Velocity.

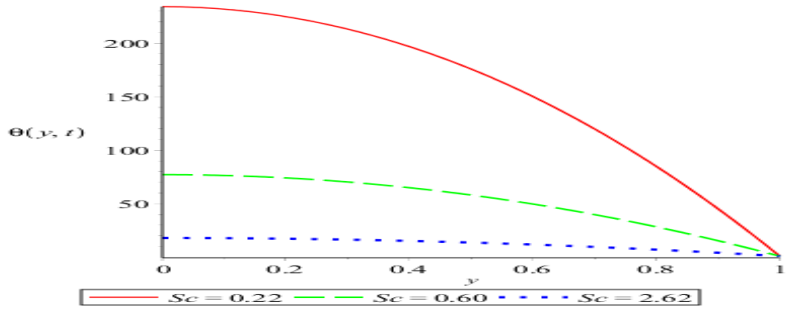


Figure 7: Schmidt Number Effect on the Temperature.

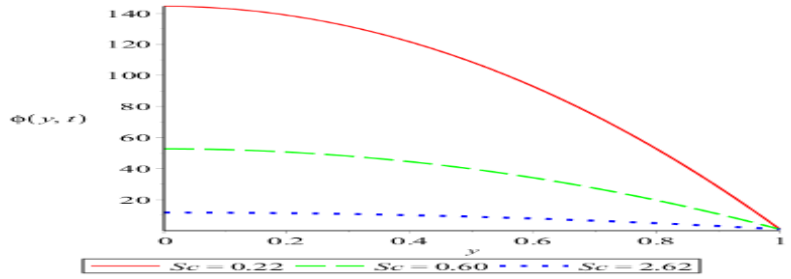


Figure 8: Schmidt Number Effect on the Concentration.

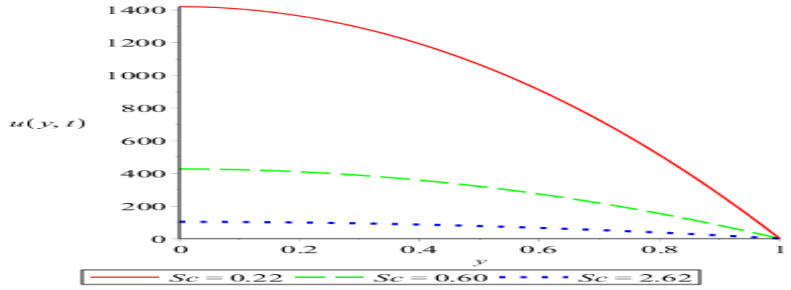


Figure 9: Schmidt Number Effect on the Velocity.

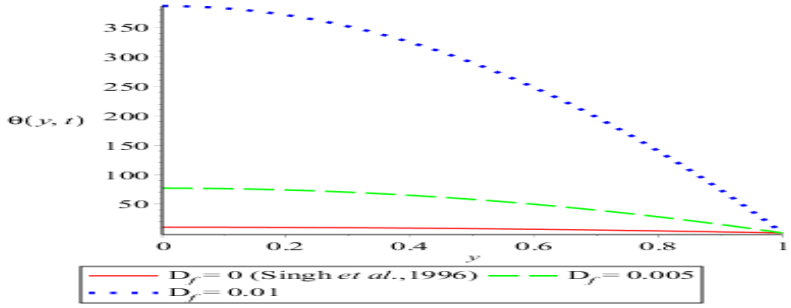


Figure 10: Dufour Effect on the Temperature.

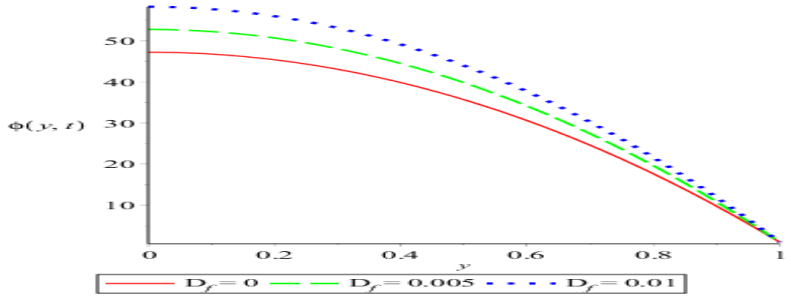


Figure 11: Dufour Effect on the Concentration.

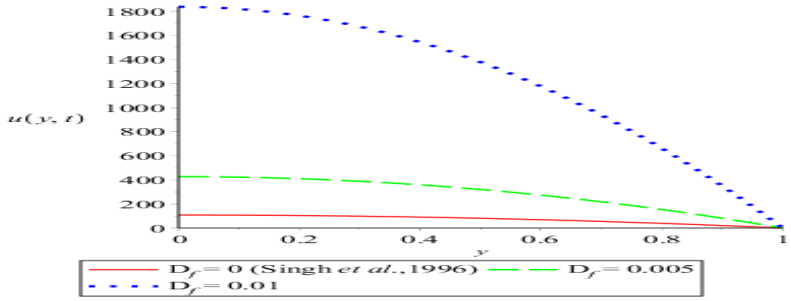


Figure 12: Dufour Effect on the Velocity.

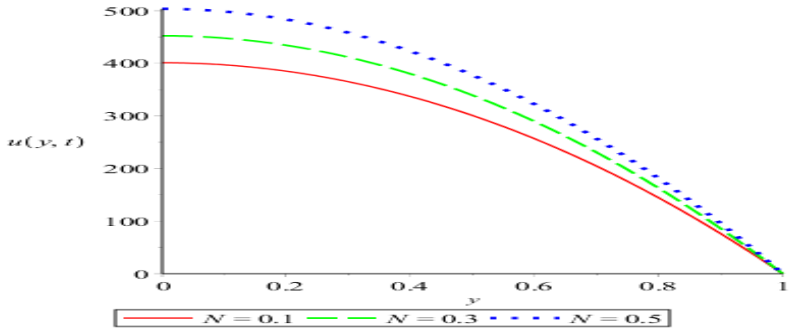


Figure 13: Buoyancy Ratio Effect on the Velocity.

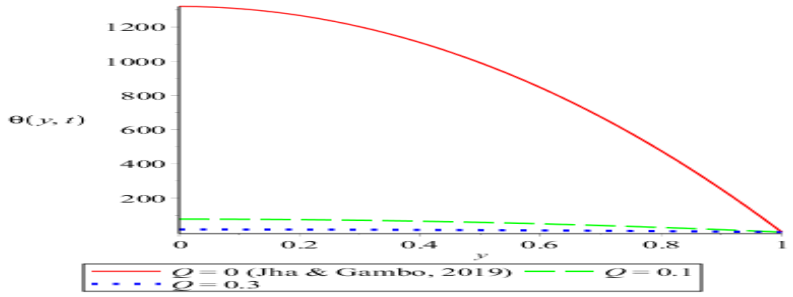


Figure 14: Heat Generation/Absorption Effect on the Temperature.

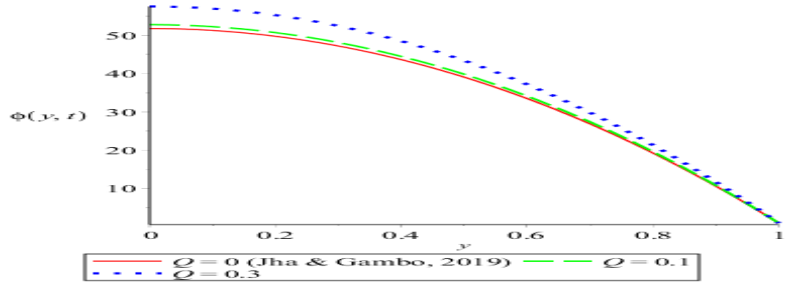


Figure 15: Heat Generation/Absorption Effect on the Concentration.

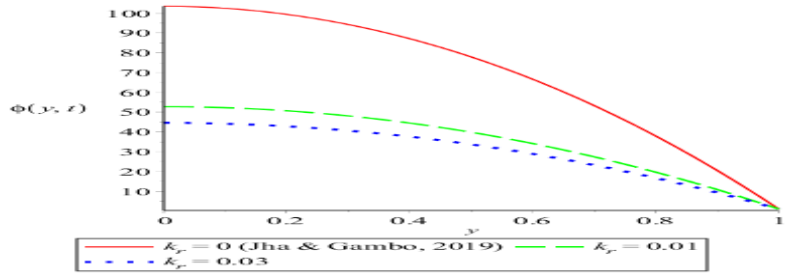


Figure 16: Chemical Reaction Effect on the Concentration.

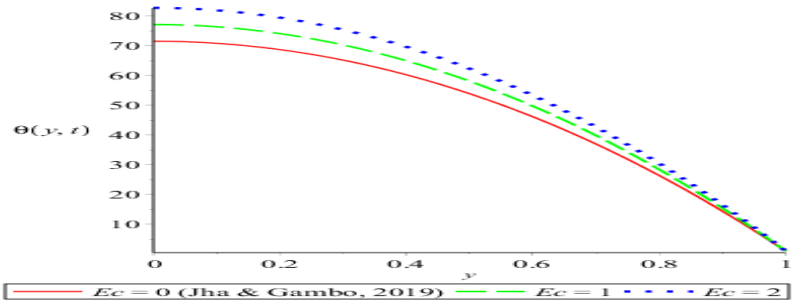


Figure 17: Eckert Number Effect on the Temperature.

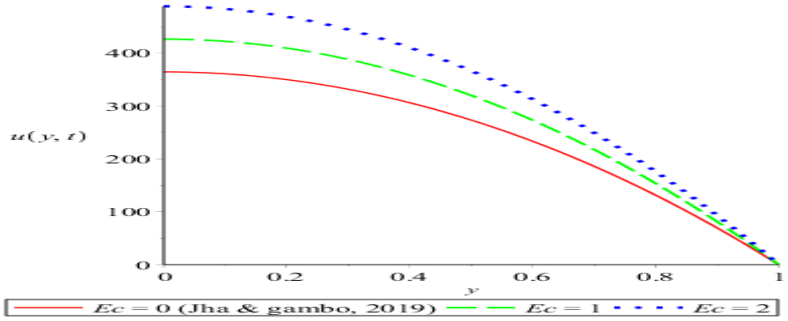


Figure 18: Eckert Number Effect on the Velocity.

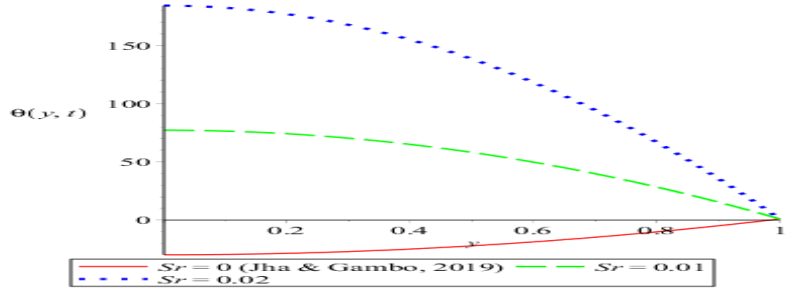


Figure 19: Soret Effect on the Temperature.

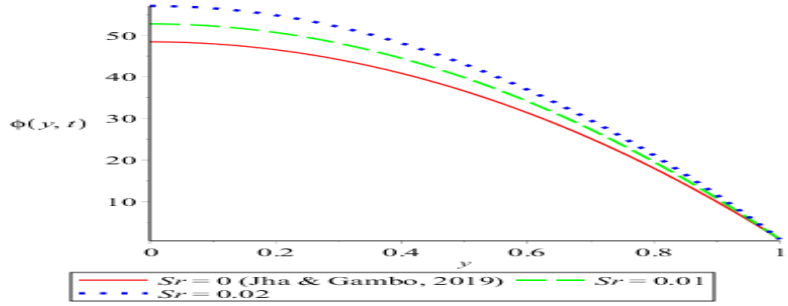


Figure 20: Soret Effect on the Concentration.

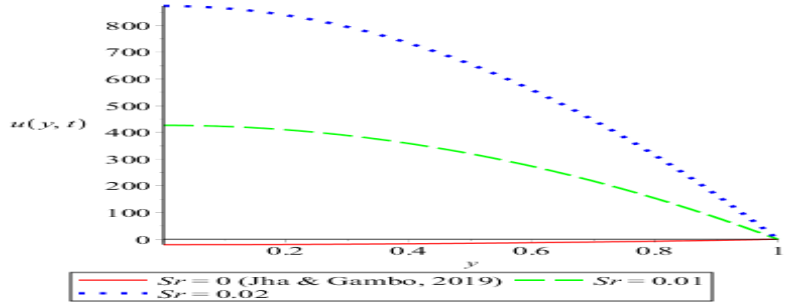


Figure 21: Soret Effect on the Velocity.

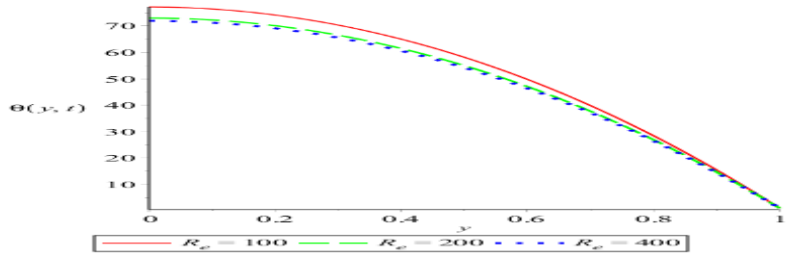


Figure 22: Reynolds Number Effect on the Temperature.

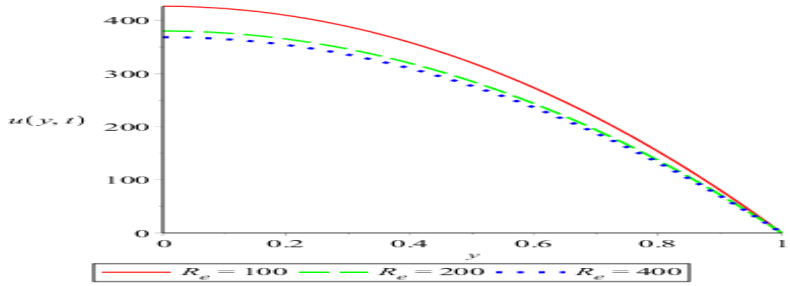


Figure 23: Reynolds Number Effect on the Velocity.

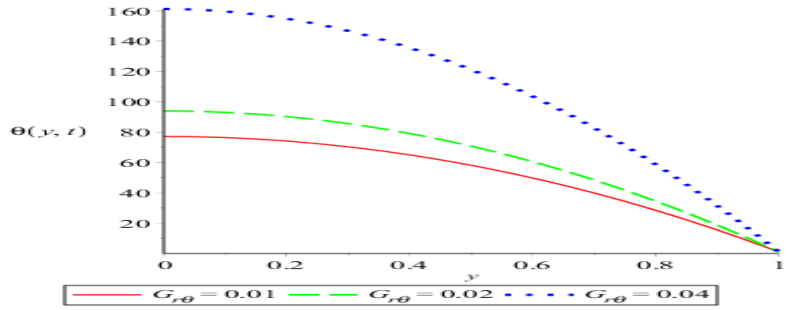


Figure 24: Thermal Grashof Number Effect on the Temperature.

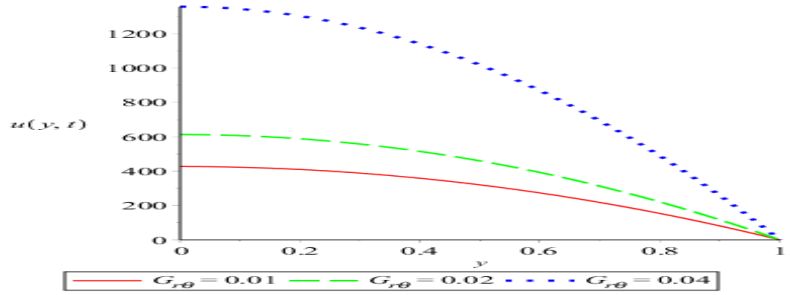


Figure 25: Thermal Grashof Number Effect on the Velocity.

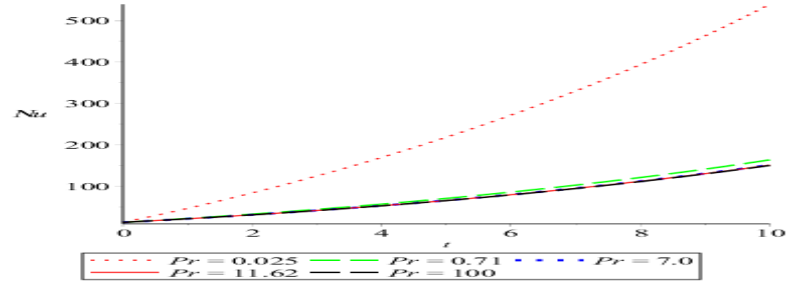


Figure 26: Nusselt Number Profile with respect to Prandtl Number.

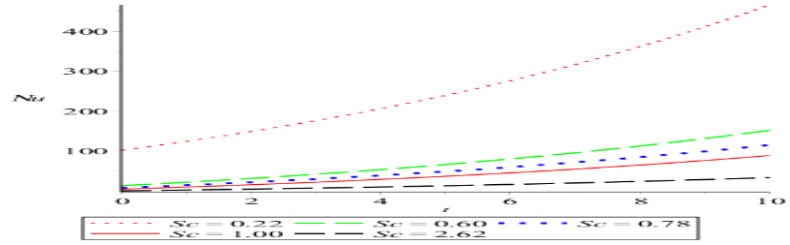


Figure 27: Nusselt Number Profile with respect to Schmidt Number.

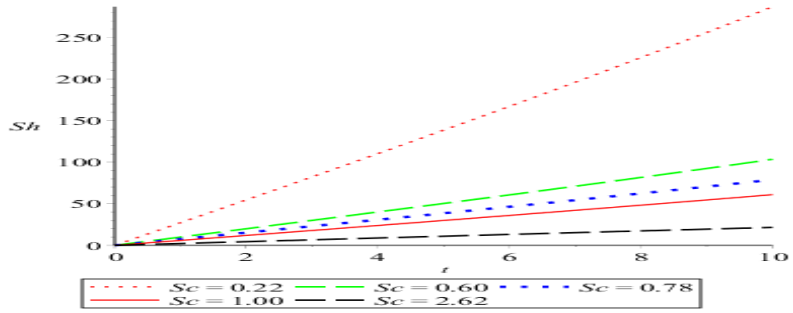


Figure 28: Sherwood Number Profile with respect to Schmidt Number.

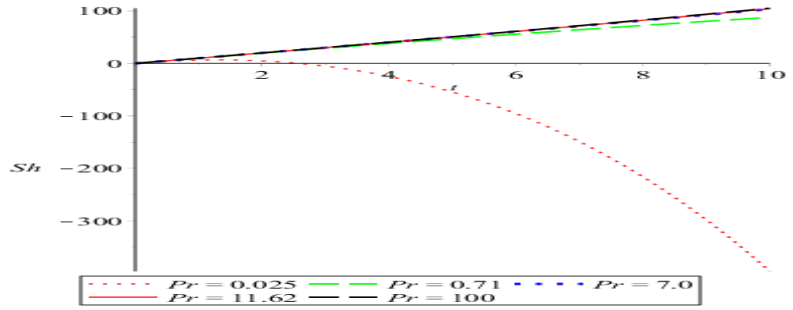


Figure 29: Sherwood Number Profile with respect to Prandtl Number.

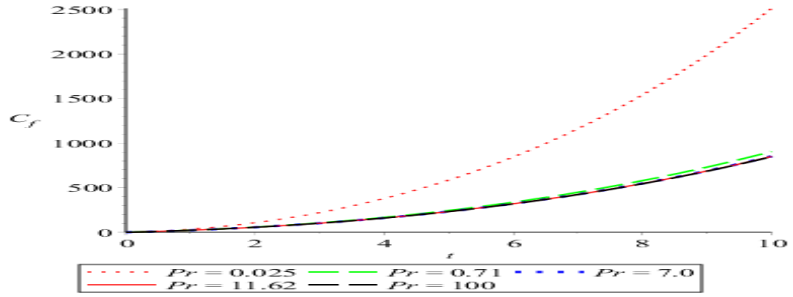


Figure30: Coefficient of Skin-friction Profile with respect to Prandtl Number.

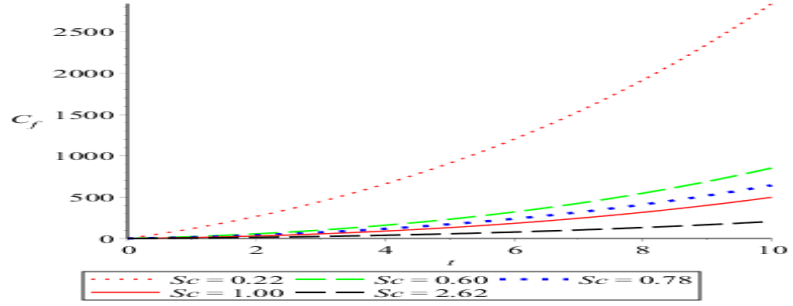


Figure 31: Coefficient of Skin-friction Profile with respect to Schmidt Number.

Discussion

Figures 1 to 3 illustrate the temporal evolution of the temperature, concentration, and velocity profiles, respectively. Figure 1. shows that the temperature increases with time and exhibits a parabolic distribution, with the maximum temperature occurring at the centre of the channel as a consequence of the symmetric heating conditions. Similarly, Figure 2 indicates an increase in concentration with time. The velocity profile presented in Figure 3 shows a more pronounced enhancement at later times, which can be attributed to the progressive strengthening of the buoyancy forces within the flow field. The three profiles therefore demonstrate the transient nature of the thermal, concentration, and hydrodynamic fields.

The effects of the Prandtl number on the temperature, concentration, and velocity fields are presented in Figures 4 to 6, respectively. An increase in the Prandtl number, ranging from 0.025 for mercury to 100 for engine oil, results in a reduction in temperature. This behaviour is associated with the lower thermal diffusivity corresponding to higher Prandtl numbers relative to momentum diffusivity, thereby limiting thermal penetration into the fluid. In contrast, the concentration increases with increasing Prandtl number because of the interaction between the thermal and concentration fields through the Soret effect. The velocity decreases as the Prandtl number increases because the reduction in temperature weakens the thermal buoyancy force. The corresponding heat-transfer behaviour is further illustrated by the Nusselt number profile in Figure 26, where

the Nusselt number decreases with increasing Prandtl number, indicating reduced heat-transfer efficiency as thermal diffusivity decreases.

The effects of the Schmidt number are presented in Figures 7 to 9, which show its influence on temperature, concentration, and velocity, respectively. As the Schmidt number increases from 0.22 for hydrogen to 2.62 for propylbenzene, the temperature decreases. This response can be attributed to the Dufour coupling between the concentration and temperature fields, whereby a reduction in mass diffusivity weakens the associated thermal transport. The concentration also decreases with increasing Schmidt number because higher Schmidt numbers correspond to lower mass diffusivity and consequently reduced species penetration. The velocity decreases as the Schmidt number increases owing to the combined reduction in temperature and concentration gradients, which weakens the buoyancy forces. The transport characteristics are further confirmed by Figures 27 and 28, which show the Nusselt number and Sherwood number profiles with respect to the Schmidt number, respectively. The corresponding skin-friction behaviour is presented in Figure 31.

The influence of the Dufour effect is presented in Figures 10 to 12, corresponding to temperature, concentration, and velocity, respectively. The limiting case considered corresponds to the work of Singh et al. (1996), in which the energy flux is not directly generated by the species concentration gradient. An increase in the Dufour number enhances the heat flux generated by concentration gradients and consequently produces a substantial increase in fluid temperature. The resulting increase in thermal buoyancy leads to an enhancement of the flow velocity. Although the concentration equation is not explicitly dependent on the Dufour parameter, changes in the temperature field influence the concentration distribution through the Soret coupling. This observation differs from the findings of Jha and Gambo (2019), who reported that concentration was independent of the Dufour effect. The present results therefore demonstrate the importance of cross-diffusion coupling in the transport process.

The effect of the buoyancy ratio is shown in Figure 13, while the effects of the heat generation/absorption parameter on temperature and concentration are presented in Figures 14 and 15, respectively. Increasing the buoyancy ratio strengthens the buoyancy forces responsible for driving the flow and consequently produces a substantial increase in velocity. The buoyancy ratio represents the relative contribution of thermal and solutal buoyancy forces to the flow. On the other hand, increasing the heat generation/absorption parameter reduces the temperature, indicating that heat absorption dominates heat generation within the range of parameters considered. The corresponding concentration increases, demonstrating the coupling between the thermal and concentration fields.

The influence of the chemical reaction parameter is depicted in Figure 16. An increase in the chemical reaction parameter significantly reduces the species concentration because a higher reaction rate results in greater consumption of the diffusing species. Thus, the chemical reaction acts as a sink for the concentration field and consequently reduces species availability within the fluid.

The effects of the Eckert number on temperature and velocity are presented in Figures 17 and 18, respectively. The Eckert number represents the effect of viscous dissipation in the flow. The limiting case corresponds to Jha and Gambo (2019), where the energy flux is not associated with viscous dissipation. Increasing the Eckert number produces a substantial increase in temperature because a greater proportion of the mechanical energy is converted into thermal energy through viscous friction. The resulting increase in temperature strengthens the thermal buoyancy forces and consequently accelerates the fluid flow. This result indicates that the conversion of mechanical energy into thermal energy becomes significant, particularly in high-velocity flows.

The Soret effect is illustrated in Figures 19 to 21, which show its influence on temperature, concentration, and velocity, respectively. The limiting case considered corresponds to Jha and Gambo (2019), where the concentration flux is not directly generated by a temperature gradient. Increasing the Soret number enhances the temperature through the cross-diffusion mechanism. The resulting temperature gradients promote mass transport, leading to an increase in concentration. The simultaneous enhancement of the temperature and concentration fields strengthens the buoyancy forces and consequently increases the flow velocity. These results confirm that the Soret and Dufour effects play important roles in double-diffusive transport systems.

The effects of the Reynolds number are presented in Figures 22 and 23, which describe its influence on temperature and velocity, respectively. Increasing the Reynolds number reduces both temperature and velocity. This behaviour can be attributed to enhanced convective transport and the associated reduction in the residence time of the fluid within the channel. The increased dominance of convective transport consequently limits thermal development and modifies the velocity distribution.

The influence of the thermal Grashof number is shown in Figures 24 and 25, representing its effects on temperature and velocity, respectively. Increasing the thermal Grashof number enhances both temperature and velocity as a result of the increased thermal buoyancy forces. A higher thermal Grashof number indicates a stronger contribution of buoyancy relative to viscous effects, thereby promoting fluid motion and enhancing the associated thermal field.

The heat and mass transfer characteristics are further examined through the Nusselt and Sherwood number profiles. Figure 26 presents the Nusselt number as a function of the Prandtl number, while Figure 27 presents the Nusselt number with respect to the Schmidt number. Figures 28 and 29 show the Sherwood number profiles with respect to the Schmidt and Prandtl numbers, respectively. The decrease in the Nusselt number with increasing Prandtl number is consistent with the reduction in thermal diffusivity and the consequent reduction in thermal penetration. Similarly, the variation of the Nusselt and Sherwood numbers with the Schmidt and Prandtl numbers demonstrates the strong coupling between heat and mass transfer in the system. These results confirm that variations in the thermal and mass diffusivities have a direct influence on the overall transport rates.

Finally, the effects of the Prandtl and Schmidt numbers on the skin-friction coefficient are presented in Figures 30 and 31, respectively. The skin-friction coefficient decreases with increasing Prandtl and Schmidt numbers. This reduction is consistent with the corresponding decrease in velocity observed in Figures 6. and 9. The results therefore establish a direct relationship between changes in the thermal and mass diffusivities and the wall shear characteristics of the flow.

Overall, the results demonstrate that the thermal, concentration, and velocity fields are strongly coupled through buoyancy, Soret and Dufour cross-diffusion, viscous dissipation, chemical reaction, and heat generation/absorption effects. The variations in the dimensionless parameters consequently produce significant

changes in heat transfer, mass transfer, fluid motion, and wall shear stress. The complete set of computed profiles, from Figures 1 to 31, provides a comprehensive representation of the combined thermal and mass-transfer behaviour of the model

Conclusion

A comprehensive mathematical model for transient double-diffusive free convection flow in a vertical channel has been developed, incorporating the combined effects of Dufour diffusion, Soret diffusion, viscous dissipation, internal heat generation/absorption, and chemical reaction under the Boussinesq approximation. The governing equations were solved analytically using Olayiwola's Generalized Polynomial Approximation Method (OGPAM) and validated numerically. The following conclusions are drawn:

i. Prandtl number effects: Increasing Prandtl number reduces fluid temperature, velocity, Nusselt number, and skin friction, while enhancing species concentration and Sherwood number.
ii. Schmidt number effects: Increasing Schmidt number reduces temperature, concentration, velocity, Nusselt number, Sherwood number, and skin friction.
iii. Dufour effect: The Dufour number significantly enhances fluid temperature, concentration, and velocity, demonstrating the importance of cross-diffusion phenomena in double-diffusive systems.
iv. Soret effect: The Soret number enhances temperature, concentration, and velocity, confirming the significant role of thermal gradients in driving mass transport.
v. Viscous dissipation: The Eckert number substantially increases both temperature and velocity, indicating that mechanical energy conversion to thermal energy is non-negligible in high-velocity flows.
vi. Buoyancy ratio: Increasing the buoyancy ratio enhances fluid velocity, underscoring the relative importance of solutal versus thermal buoyancy forces.
vii. Heat generation/absorption: The heat source parameter reduces temperature while enhancing concentration, demonstrating the complex coupling between thermal and concentration fields.
viii. Chemical reaction: Increasing the chemical reaction parameter reduces species concentration, as expected for reactive systems.
ix. Reynolds number: Increasing Reynolds number reduces both temperature and velocity due to enhanced convective effects.
x. Thermal Grashof number: Increasing thermal Grashof number enhances both temperature and velocity through strengthened buoyancy forces.

The results have immediate relevance to practical applications including isotope separation, cooling of vertical printed circuit boards, geothermal system design, chemical processing equipment, and environmental management systems. The analytical solutions provide efficient tools for parametric studies and system optimization.

Funding

This study received funding from TETFund through the Institutional Based Research (IBR) grant.

Nomenclature

C' is the fluid specie concentration,
C_0' is the fluid specie concentration near the wall $y' = 0$,
C_L' is the fluid specie concentration near the wall $y' = L$,
D_m is the coefficient of mass diffusivity,
K_T is the coefficient of thermal diffusion,
$K_C{}^*$ is the chemical reaction parameter,
T' is the fluid temperature
D is the diffusion coefficient,
T_0' is the wall temperature at $y' = 0$,
T_L' is the wall temperature at $y' = L$,
D^* is the dimensional Dufur parameter $\left(D^* = \frac{\rho D_m K_T}{C_s \rho C_p}\right)$
K^* is the dimensional Soret parameter $\left(K^* = \frac{D_m K_T}{T_m}\right)$
v is the kinematic viscosity,
T_m is the mean fluid temperature,
C_p is the specific heat capacity,
Q^* is the heat source parameter,
C_s is the concentration susceptibility,
u' is the fluid velocity,
g is the gravitational acceleration,
t' is the dimensional time,
x' is the axis along the wall,
y' is the axis perpendicular to the wall,
t_0 is the ramped time.
α is the coefficient of thermal diffusivity $\left(\alpha = \frac{K}{\rho C_p}\right)$,
β is the coefficient of thermal expansion,
β^* is the coefficient of concentration expansion,
ρ is density,
K is the thermal conductivity,
v is the kinematic viscosity,
θ is dimensionless temperature
ϕ is dimensionless concentration

REFERENCES

Alam, M. S., Rahman, M. M., Ferdows, M., Kaino, K., Mureithi, E. & Postelnicu, A. (2007). Diffusion-Thermo and Thermal-Diffusion Effects on Free Convective Heat and Mass Transfer Flow in a Porous Medium with Time Dependent Temperature and Concentration. *Int. J. Appl. Eng. Res.*, 2, 81–96.

Chanson, H. (2020). The Hydraulics of Open Channel Flow: An Introduction (3rd ed.). Elsevier.

Ibrahim A. & Musa A.O. (2023). On the Performance of Sarima and Sarimax model forecasting monthly Average Rainfall in Kogi state, Nigeria. FUDMA Journal of Sciences (FJS), Vol. 7, No. 6, pp 24–31 https://doi.org/10.33003/fjs-2023-07062-2095S

Ismael, M. A., Pop, I. & Chamkha, A. J. (2014). Mixed convection in a lid-driven square cavity with partial slip. *Int. J. Sci.*, *82*, 47–61.

Jha, B. K. & Gambo, Y. Y. (2019). Dufour Effect with Ramped Wall Temperature and Specie Concentration on Natural Convection Flow through a Channel. Physics, 1, 111–130.

Meyer, J. R. & Rogers, R. P. (2022). Transient flow analysis in vertical channels: A comprehensive review. *Fluid Dynamics Research*, 54(3), 034501.

Nash, J. C. & Morris, R. C. (2018). Modeling and management of transient flow in hydraulic systems. *Hydraulic Engineering Journal*, 32(4), 145-161.

Olayiwola, R. O. (2022). Solving parabolic equations by Olayiwola's generalized polynomial approximation method. *International Journal of Mathematical Analysis and Modelling*, 5(3), 24–43.

Patankar, S. V. (2020). Numerical Heat Transfer and Fluid Flow (2nd ed.). CRC Press.

Singh, A. K., Gholami, H. R. & Soundalgekar, V. M. (1996). Transient free convection flow between two vertical parallel plates. *Heat Mass Transfer,* 31, 329–333.

Umavathi, J. C. & Sheremet, M. A. (2016). Mixed convection flow of an electrically conducting fluid in a vertical channel using Robin boundary conditions with heat source/sink. *Eur. J. Mech. B/Fluids,* 55, 132–145.

Umavathi, J.C., Sheremet, M. & Mohiuddin, S. (2016). Combined effect of variable viscosity and thermal conductivity on mixed convection flow of a viscous fluid in a vertical channel in the presence of first order chemical reaction. *Eur. J. Mech. B/Fluids,* 58, 98–108.

Yahaya, J. D., Agbata, B. C., Oyeyemi, O. R., Raji, M., Adaji, I., Yusuf, D. A., & Senewo, E. O. (2025). Unsteady dean flow of dusty fluids between two oscillating cylinders. *Proceedings of the Nigerian Society of Physical Sciences*, 157-157.

Appendix: Coefficients for OGPAM Solutions

The coefficients appearing in equations (25) and (27) are defined as follows:

$$C_9 = 3b\left(1-\frac{C_1}{Q}\right),\ C_{10} = 3bC_4,\ C_{11} = 3bC_5$$

$$C_{12} = \frac{2aGr_\theta C_6 C_7^2}{Re^2} - \frac{3D_f C_9}{K_r},\ C_{13} = \frac{4C_3 C_6 aGr_\theta}{Re^2}, C_{14} = \frac{2aGr_\theta C_3^2}{Re^2}$$

$$C_{15} = \frac{4aGr_\theta C_6 C_7}{Re^2} - \frac{3D_f C_{10}}{Q+K_r}, C_{16} = 3D_f\left(\frac{C_{10}}{Q+K_r} - \frac{C_9}{K_r}\right) - \frac{4aGr_\theta C_6 C_8}{Re^2}$$

$$C_{16} = 3D_f\left(\frac{C_{10}}{Q+K_r} - \frac{C_9}{K_r}\right) - \frac{4aGr_\theta C_6 C_8}{Re^2}, C_{17} = \frac{4aGr_\theta C_3 C_7}{Re^2},\ C_{18} = \frac{4aGr_\theta C_3 C_7}{Re^3} + 3D_f C_{11}$$

$$C_{19} = \frac{2aGr_\theta C_7^2}{Re^2},\ C_{20} = \frac{4aGr_\theta C_7 C_8}{Re^2},\ C_{21} = \frac{2aGr_\theta C_8^2}{Re^2}, C_{22} = -\left(\frac{C_{12}}{Q} + \frac{C_{13}}{Q^2} + \frac{2C_{14}}{Q^3}\right)$$

$$C_{23} = -\left(\frac{C_{13}}{Q} + \frac{2C_{14}}{Q^2}\right)$$

$$C_{24} = -\frac{C_{14}}{Q},\ C_{25} = \frac{C_{12}}{Q} + \frac{C_{13}}{Q^2} + \frac{2C_{14}}{Q^3} + \frac{C_{16}}{Q+K_r} - \frac{C_{19}}{Q} - \frac{C_{20}}{K_r} - \frac{C_{18}}{(Q+K_r)^2} - \frac{C_{21}}{Q+2K_r}$$

$$C_{26} = \frac{C_{18}}{(Q+K_r)^2} - \frac{C_{16}}{Q+K_r},\ C_{27} = C_{15},\ C_{28} = \frac{C_{18}}{Q+K_r}$$

$$C_{29} = \frac{C_{17}}{2},\ C_{30} = \frac{C_{19}}{Q},\ C_{31} = \frac{C_{20}}{K_r},\ C_{32} = \frac{C_{21}}{Q+2K_r}$$

$$C_{33} = \frac{1}{2} + C_{22} + \frac{C_0}{K_r},\ C_{34} = C_{26} + \left(1+\frac{C_0}{K_r}\right)$$

where:

$$C_3 = \frac{1}{2} - \frac{C_1}{Q},\ C_4 = 1 + \frac{C_1}{Q} - \frac{C_2}{Q+K_r},\ C_5 = \frac{C_2}{Q+K_r}, C_6 = \frac{2aGr_\theta}{Re^2},\ C_7 = \frac{C_4}{Q},\ C_8 = \frac{C_5}{K_r}$$

©2026 This is an Open Access article distributed under the terms of the Creative Commons Attribution 4.0 International license viewed via https://creativecommons.org/licenses/by/4.0/ which permits unrestricted use, distribution, and reproduction in any medium, provided the original work is cited appropriately.